Proceedings of the 10th World Congress on Civil, Structural, and Environmental Engineering (CSEE 2025)
Barcelona, Spain - April, 2025
Paper No. ICSECT 178
DOI: 10.11159/icsect25.178

Numerical Simulation of the Pullout Behavior of Steel Fiber Composite Bars (SFCB) Embedded in Concrete

Haya Zuaiter[1], Doha ElMaoued[1], Mohammad AlHamaydeh[1], Mohamed Elkafrawy[1]
[1] American University of Sharjah
PO Box 26666, Sharjah, UAE
g00102524@aus.adu; g00102501@aus.edu; malhamaydeh@aus.edu; melkafrawy@aus.edu

Abstract **-** Steel fiber composite bars (SFCB) are a promising alternative to steel and fiber-reinforced polymer (FRP) reinforcement due to their high elastic modulus and tensile strength, impressive ductility, and outstanding corrosion resistance. This research investigates the impact of increasing the diameter of the inner steel bar of a glass SFCB on the bond stress between the bar and the surrounding concrete. Abaqus finite element software simulates the pullout behavior between glass SFCB and normal-strength concrete. Results of the FE models were compared with experimental results in terms of crack patterns and bond stresses. The FE model results correlated well with the experimental results having a 0.54% error in the ultimate bond stress and a 0.67% error in the corresponding slip. A parametric study is conducted in which the diameter of the inner steel core is increased while all other material properties and boundary conditions remain constant. The composite material's behavior is analyzed accounting for the interactions between the steel bar, glass FRP (GFRP) cover, and surrounding concrete. Notably, increasing the diameter of the inner steel bar from 8.6 mm to 12.6 mm increases the bond stress from 20.7 MPa to 25.1 MPa and increases the ultimate slip from 1.17 mm to 1.57 mm. The increase in ultimate slip is due to the rise in bond stress which in turn is due to a decrease in the radial confinement stress between the SFCB and the surrounding concrete.

Keywords**:** Pullout behavior, Concrete, SFCB, Bond stress, Slip, Numerical Simulation

1. Introduction

Reinforced concrete often suffers from corrosion of embedded steel reinforcement, particularly in harsh environments like coastal areas with wet-dry cycles and tidal effects [1], [2]. This leads to cracks, spalling, and reduced load-bearing capacity due to loss of bond between steel and concrete [3]–[5]. Fiber Reinforced Polymer (FRP) bars offer corrosion resistance but are brittle and costly [4], [6]. To address these issues, researchers developed Steel Fiber Composite Bars (SFCBs), combining steel's ductility with FRP's corrosion resistance, offering superior strength, ductility, and compressibility compared to either material alone [7]–[9].

Bond stress between reinforcement and concrete decreases with larger bar diameters, longer embedment lengths, or increased air entrapment during curing [10]–[14]. Self-compacting concrete (SCC) shows better bond stress than conventional vibrated concrete (CVC) for small-diameter bars, though this advantage diminishes with larger diameters [11]. Studies indicate that ribbed steel bars exhibit higher bond stress than FRP or SFCBs [15]–[18]. However, excessive slip of SFCBs can reduce structural performance, emphasizing the need to enhance their bond behavior [19], [20].

Research on SFCBs reveals mixed findings: wrapping steel with FRP reduces bond stress compared to unwrapped steel, but increasing the steel core diameter improves bond stress for glass SFCBs [9]. Conversely, thicker basalt layers around a constant-diameter steel core decrease bond stress [21]. This inconsistency in results can be attributed to different material properties, geometric configuration, test setup, and environment, as well as loading rate [22]–[28].

This study aims to numerically investigate how varying the inner steel core diameter of glass SFCBs impacts bond stress with concrete [29]. It also explores the feasibility of using glass SFCBs in reinforced concrete elements, addressing critical factors affecting their bond performance and structural integrity [3], [9].

2. Finite Element (FE) Model

2.1. Description of the model

This study investigates the bonding behavior between concrete and SFCB in pullout samples. Pullout samples consist of concrete cubes reinforced with SFCB. SFCB is embedded into concrete with an embedment length five times its total diameter. The total diameter is obtained by adding the steel bar diameter to the GFRP thickness. In this study, the total diameter of SFCB varies across pullout samples while the dimensions of the concrete cube remain constant. Therefore, the embedment lengths across pullout samples vary. Fig 1 shows the geometry of the pullout sample. The numerical program was developed for three pullout samples including POT-12, POT-14, and POT-16 to investigate the influence of total bar diameter of SFCB on the bond behavior. POT – T12 stands for a pullout sample with a 12 mm total diameter of which 8.3 mm is steel bar and 4 mm is GFRP sheet. Table 1. summarizes the specifications of pullout samples.

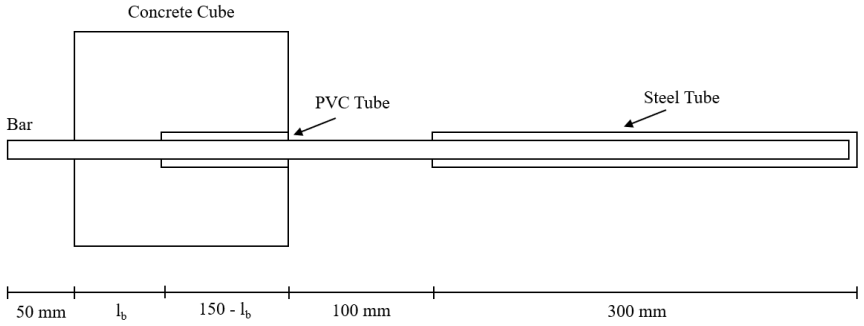

Fig 1: Pullout sample geometry

Table 1: Specifications of pullout samples

Pullout sample	Steel bar diameter (mm)	GFRP thickness (mm)	Total bar diameter (mm)	Bonded bar length, l_b (mm)
POT-12	8.3	4	12.6	63
POT-14	10.3	4	14.6	73
POT-16	12.3	4	16.6	83

2.2. Material Properties

2.2.1 Concrete

The mechanical behavior of concrete is simulated with the Concrete Damage Plasticity (CDP) model in ABAQUS. Constitutive laws in the CDP model are utilized to find the compressive and tensile behavior of concrete. Dilatation angle and viscosity parameters are fixed at 38.5 and 0.008 to describe the plastic flow potential of concrete. The compressive behavior is defined using Hognestad's model [30] to capture the nonlinear behavior of concrete under compression. Similarly, the tensile behavior is defined using Hsu and Mo's model [31] to capture the nonlinear behavior of concrete under tension. In this study, compressive strength f'_c is taken as 38.4 MPa based on the experimental work done by Xu et al [32].

Hognestad's model [30]

$$f_c = f'_c\left[\frac{2\varepsilon_c}{\varepsilon_{co}} - \left(\frac{\varepsilon_c}{\varepsilon_{co}}\right)^2\right] \text{ when } 0 \le \varepsilon_c \le \varepsilon_{co}$$

$$f_c = f'_c\left[1 - 0.15\left(\frac{\varepsilon_c - \varepsilon_{co}}{\varepsilon_{cu} - \varepsilon_{co}}\right)\right] \text{ when } \varepsilon_{cu} \le \varepsilon_c \le \varepsilon_{co}$$

where $\varepsilon_{co} = \frac{2f'_c}{E_c}$ and $E_c = 12680 + 460f'_c$

Hsu and Mo's model [31]

$$f_t = E_c\varepsilon_t \quad \text{when } \varepsilon_t \le \varepsilon_{cr}$$

$$f_t = f_r\left(\frac{\varepsilon_{cr}}{\varepsilon_t}\right)^n \quad \text{when } \varepsilon_t \le \varepsilon_{cr}$$

where $f_r = 0.33\sqrt{f'_c}$ and $\varepsilon_{cr} = \frac{f_r}{E_c}$

2.2.2 Steel Bar

The steel bar is modeled as an elastic perfectly plastic material that deforms elastically until the yield strength. Beyond the yield strength, the material deforms plastically at a constant value. The modulus of elasticity is defined as 200 GPa and the poissons ratio is 0.3. The properties of steel bars, including the yield strength and ultimate strength, vary according to the

bar diameter [33]. In this study, steel bar diameters of 8.6 mm, 10.6 mm, and 12.6 mm have yield strength values of 477.7 MPa, 426 MPa, and 440 MPa and ultimate strength values of 687.6 MPa, 667 MPa, and 673 MPa, respectively [32].

2.2.3 GFRP

Due to its orthotropic nature, the mechanical properties of GFRP vary in all directions of the coordinate system [34]–[36]. The mechanical properties of GFRP defined in the model are adopted from Alhayek et al [37]. The longitudinal elastic modulus along the x direction is 36.3 GPa, which shows high stiffness in the direction of the fibers. The transverse moduli in the y and z directions are much lower at 10.8 GPa since these directions rely on the polymer matrix rather than the fibers. The poissons ratio in the xy and xz planes is defined as 0.28, while 0.09 for the yz plane. The shear moduli in the xy and xz planes are 4 GPa. The longitudinal tensile strength along the x direction is 596 MPa, which gives the high loading-carrying ability of the GFRP along the direction of the fiber.

2.3. Mesh and Boundary Conditions

The model is discretized using 4-node bilinear axisymmetric quadrilateral elements (CAX4). Mesh sensitivity analysis was conducted to determine the most suitable mesh size that achieves a reasonable compromise between computational efficiency and accuracy. The optimal element mesh size is determined by reducing the size until the desired accuracy is achieved for the desired application of the model [38]–[40]. After several iterations, a mesh size of 5 mm was determined to be the most suitable. To account for symmetry, a vertical roller boundary condition is placed at the symmetric line. A roller boundary condition is applied to the top and bottom concrete faces to restrict vertical movements. An upward displacement is applied to the steel tube around SFCB to simulate the pullout loading.

3. Results and Discussion

The bonding strength between the bar and concrete in pullout samples influences their cracking patterns and failure modes. Studies have shown that bar pullout mainly occurs when the bond is weak, while bar rupture and concrete splitting occur when the bond is strong. Under pullout loading, the stress transfer in concrete reinforced with SFCB is more complicated than in concrete reinforced with pure steel bars. This is because the steel core in SFCB transfers the stress to the fiber layer first and then to the surrounding concrete. Fibers exert shear and radial stresses on the surrounding concrete with shear stresses acting along the bonding interface between fibers and concrete and radial stresses acting perpendicular to the bonding surface.

The FE model was validated against the experimental results presented by Xu et al. [32] for the pullout sample with conventional concrete. The validation of the FE model is based on the bond stress versus slip responses and failure mode. The bond stress is obtained from the shear forces at the concrete-SFCB interface, whereas the slip is obtained at a point on the shorter side of the bar. Fig. 2 shows the bond stress versus slip response of the FE model in comparison to the experimental response. Results from the FE model correlated well with the experimental response, achieving ultimate bond stress of 20.554 MPa at 0.775 mm as compared to 20.665 MPa at 0.781 mm in the experimental response. The percentage error of the ultimate bond strength is 0.54% while the corresponding slip percentage error is 0.76%. The primary failure mode observed in the FE model is concrete splitting which correlates with the experimental failure mode shown in Fig. 3. Under pullout loading, deformations progressed from the anchorage point between concrete and SFCB towards the middle of the cube, causing concrete to split.

The bonding behavior between concrete and SFCB in the FE model is mainly controlled by stiffness and damage initiation parameters. Stiffness parameters include normal stiffness of the interface (Knn) and shear stiffness of the interface (Kss and Ktt). Damage initiation is characterized by normal, shear 1, and shear 2, in terms of the maximum nominal stress or strain in each direction. The damage initiation criterion is characterized by a quadratic interaction function of nominal stress ratios. To achieve high accuracy, thousands of simulations were performed with Python scripts for automating parameter identification. This approach successfully captured the acquired parameters in agreement with the experimental work within an error of less than 1%.

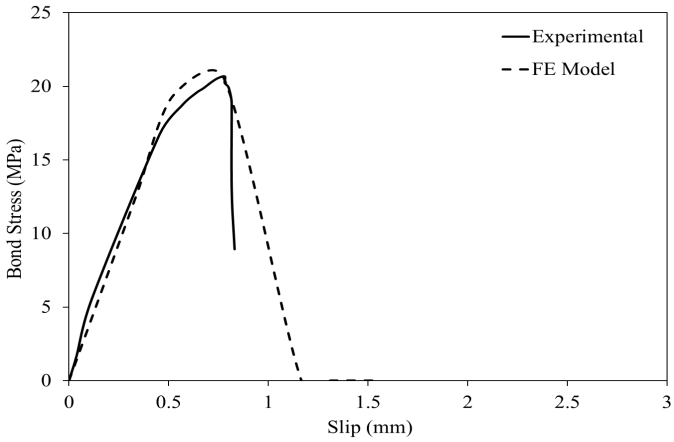

Fig. 2: Validation of the FE model

(a) (b)

Fig. 3: Cracking pattern (a) FE model (b) Experimental sample [32]

As seen in Fig 4, there is a clear correlation between the diameter of the steel bar embedded within the glass SFCB and the bond stress that develops between the reinforcement and the surrounding concrete. For instance, the SFCB with a diameter of 12.6 mm, having a steel bar measuring 8.6 mm in diameter, has a bond stress of 20.7 MPa at a corresponding slip of 0.78 mm. Increasing the steel bar diameter to 10.6 mm to have a SFCB of 14.6 mm increases the bond stress by 12% to 23.1 MPa and the corresponding slip to 0.78 mm. Finally, further increasing the diameter of the SFCB to 16.6 mm where the inner steel bar has a diameter of 12.6 mm, increases the bond stress till it reaches 25.1 MPa and the corresponding slip is 0.78 mm. Increasing the diameter of the inner steel core while maintaining a constant thickness of the GFRP outer layer, simultaneously increases the bond stress of the SFCB whereas the corresponding slip is relatively constant. This is because an increase in the diameter of the steel bar decreases the radial confinement stress. This refers to the compressive stress that the FRP outer layer exerts on the steel inner core or the stress that the FRP layer applies on the surrounding concrete. This radial confinement stress is influenced by the radius of the steel core, the radius of the FRP cover, the pressure at the interface between the materials, the elastic modulus of FRP, and the Poisson ratio of steel. When the thickness of the GFRP layer is constant, increasing the diameter of the steel bar decreases the radial confinement effect. As a result, there is less stress acting by the GFRP on the steel and on the concrete which in turn increases the bond stress.

The ultimate slip or the slip at failure of the SFCB is greater than that of pure steel bars. In this analysis, the ultimate slip ranges between 1.17mm for the SFCB with the smallest diameter and 1.57 mm for the SFCB with the largest diameter. This ultimate slip is the slip at which the bond between the reinforcement and the surrounding concrete fails. As the ultimate slip increases for specimens with higher bond stress, this means that the interaction area carries a significant load and absorbs a large amount of energy prior to failure. The GFRP cover enhances the bar's slip capacity. Although the thickness of the GFRP remains constant throughout the study, increasing the diameter of the inner steel bar increases the total diameter of

the SFCB which in turn means an increase in the ultimate slip. Therefore, a high ultimate slip reflects a strong bond between the SFCB and the concrete.

Von Mises Stresses is an important parameter to study in numerical models [41]–[45]. These stresses show the deformability of a material under complex loading conditions. Fig 5 clearly shows that increasing the diameter of the inner steel core of the glass SFCB decreases the maximum Von Mises Stress experienced by the rebar. The 12.6 mm glass SFCB has the largest maximum Von Mises stress at around 43.34 MPa. When the diameter of the glass SFCB increases to 14.6 mm, the maximum Von Mises Stress reduces to 7.59 MPa, and it further decreases to 1.61 MPa when the diameter is 16.6 mm. A high Von Mises Stress at the interface of the SFCB and the concrete indicates that the region is under severe internal stresses, which potentially lead to yielding, plastic deformation, or failure. Therefore, high Von Mises Stresses occur in SFCB of small diameters where the bond stress between the bar and the concrete is minimal. As the diameter of the internal steel bar increases, the distribution of stress around the bar becomes more uniform. This results in a reduction of localized stress concentrations which in turn prevents failure.

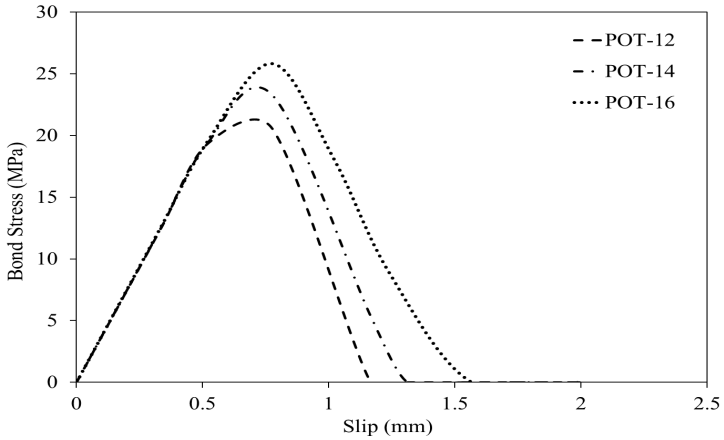

Fig. 4: Parametric study

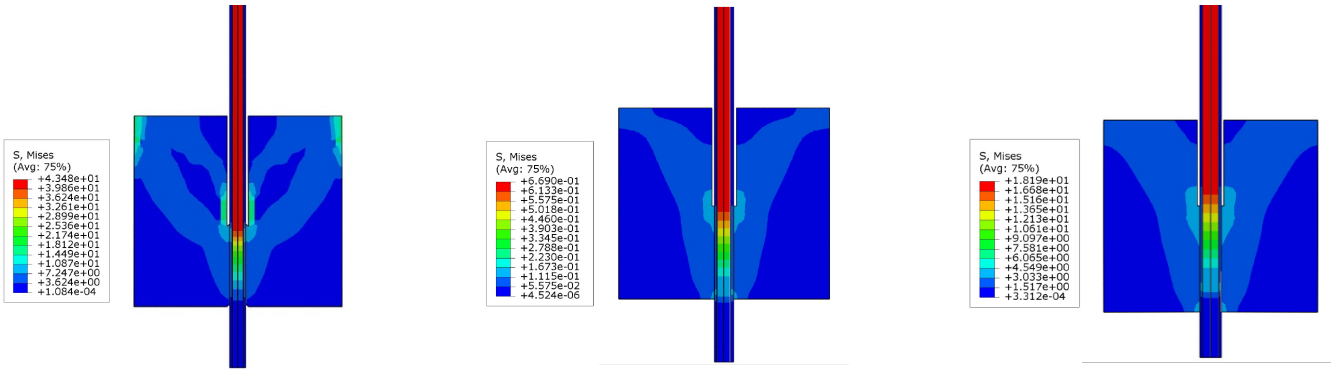

(a) (b) (c)

Fig 5: Von Mises Stresses of (a) POT-12 (b) POT-14 (c) POT-16

4. Conclusion

Reinforced concrete structures are susceptible to durability challenges in harsh environments. Durability challenges arise from the corrosion of steel reinforcement and degradation of concrete causing cracking, spalling, and ultimately structural failure. Glass SFCB emerged as an attractive alternative to steel bars in reinforced concrete elements. The pullout behavior between concrete and SFCB has been studied, and the following conclusions have been reported.

1. The validation of the FE model in terms of bond versus slip response and failure mode correlated well with the experimental results with an error of 0.54% in ultimate bond stress and 0.76% in slip measurements. Due to material properties differences, the FE model had a higher energy absorption capacity.

2. Increasing the steel bar diameter in glass SFCB from 8.6 mm to 10.6 mm and 12.6 mm resulted in a slight increase in the bond stress by 12% and 8.5% respectively, whereas the corresponding slip remains approximately constant at 0.775 to 0.778 mm. This is mainly due to the reduced radial confinement stress that the FRP layer applies on the surrounding concrete.
3. The ultimate slip at which the bond between concrete and SFCB fails increases from 1.166 mm to 1.567 mm, enabling pullout samples to have more ductility and resilience. Higher ultimate slip indicated better bonding performance that results in a higher energy absorbing capacity.
4. Von Mises stresses reduce with the increase in steel bar diameter from 43.34 MPa, 7.59 MPa, and 1.61 MPa with the increase in bar diameter from 12.6 mm, 14.6 mm, to 16.6 mm. This indicates diminished localized stress concentration and improved resistance to failure. Larger steel bar diameters reduce stresses more evenly at the interface which reduces concentration points.

Acknowledgements

This research was financially supported by the American University of Sharjah (AUS) through the Faculty Research Grant program (FRG23-E-E42 and FRG22-C-E20). The authors greatly appreciate this financial support. This paper represents the opinions of the authors and does not intend to represent the position or opinions of AUS.

References

[1] M. Otieno, H. Beushausen, and M. Alexander, "Chloride-induced corrosion of steel in cracked concrete – Part I: Experimental studies under accelerated and natural marine environments," *Cem Concr Res*, vol. 79, pp. 373–385, 2015.

[2] Y. Wang, Y. Zhong, B. Wan, B. Zhang, Z. Wei, and Y. Bai, "Axial compressive behavior and modeling of fiber-reinforced polymer-concrete-steel double-skin tubular stub columns with a rectangular outer tube and an elliptical inner tube," vol. 260, p. 114222, 2022.

[3] L. Xu, X. Wang, J. Pan, J. Zhou, and W. Liu, "Bond behavior between steel-FRP composite bars and engineered cementitious composites in pullout conditions," *Eng Struct*, vol. 299, Jan. 2024, doi: 10.1016/j.engstruct.2023.117086.

[4] J.-P. Won, C.-G. Park, and C.-I. Jang, "Tensile Fracture and Bond Properties of Ductile Hybrid FRP Reinforcing Bars," *Polymers & Polymer Composites*, vol. 15, no. 1, 2007.

[5] H. Yalciner and A. Kumbasaroglu, "Experimental Study to Predict Bond-Slip Behavior of Corroded Reinforced Concrete Columns," *ACI Struct J*, vol. 119, no. 5, pp. 111–128, 2022.

[6] G. Ma, Y. Huang, F. Aslani, and T. Kim, "Tensile and bonding behaviours of hybridized BFRP–steel bars as concrete reinforcement," *Constr Build Mater*, vol. 201, pp. 62–71, Mar. 2019, doi: 10.1016/j.conbuildmat.2018.12.196.

[7] G. Wu, Z. Y. Sun, Z. S. Wu, and Y. B. Luo, "Mechanical Properties of Steel-FRP Composite Bars (SFCBs) and Performance of SFCB Reinforced Concrete Structures," *Advances in Structural Engineering*, vol. 15, no. 4, pp. 625–635, 2016.

[8] Y.-C. Guo, S.-H. Xiao, J.-J. Zeng, J.-Y. Su, T.-Z. Li, and Z.-H. Xie, "Behavior of concrete-filled FRP tube columns internally reinforced with FRP-steel composite bars under axial compression," *Constr Build Mater*, vol. 315, p. 125714, 2022.

[9] B. Basaran and E. T. Donmez, "Investigation of Bond Strength Between GFRP Wrapped Steel Reinforcement and Concrete with Pullout Test," *Hittite Journal of Science and Engineering*, vol. 7, no. 4, Dec. 2020.

[10] R. Mathey and D. Watstein, " Investigation of bond in beam and pull out specimens with high yield strength deformed bars," *ACI Journal*, no. 57, pp. 1071–1089, 1961.

[11] P. Desnerck, G. De Schutter, and L. Taerwe, " Bond behaviour of reinforcing bars in self-compacting concrete: experimental determination by using beam tests," *Mater Struct*, no. 43, pp. 53–62, 2010.

[12] N. Sai Teja, G. Madhuri, and P. Veerabhadra Rao, "Investigation of Bond Strength in Concrete Embedded with Steel Rebar Attached To Coupler Using Pull-Out Test ," *Int J Innov Res Sci Eng Technol*, vol. 6, no. 8, 2017.

[13] E. Tuğrul Tunç, K. Esat Alyamaç, R. İnce, and Z. Çınar Ulucan, "Relationship between Reinforcement Diameter and Bond Stress in High Performance Lightweight Concrete ," *European Journal of Science and Technology*, no. 23, pp. 851–860, 2021.

[14] G. Appa Rao, "PARAMETERS INFLUENCING BOND STRENGTH OF REBARS IN REINFORCED CONCRETE ," *International Journal of Applied Engineering and Technology I*, vol. 4, no. 1, pp. 72–81, 2014.
[15] W. Ge, M. Han, Z. Guan, P. Zhang, A. Ashour, W. Li, W. Lu, D. Cao, and S. Yao, "Tension and bonding behaviour of steel-FRP composite bars subjected to the coupling effects of chloride corrosion and load," *Constr Build Mater*, vol. 296, p. 123641, 2021.
[16] M. Harajli and M. Abouniaj, "Bond performance of GFRP bars in tension: Experimental evaluation and assessment of ACI 440 guidelines," *Journal of Composites for Construction*, vol. 14, no. 6, pp. 659–668, 2010.
[17] J.-Y. Lee, T.-Y. Kim, T.-J. Kim, C.-K. Yi, J.-S. Park, Y.-C. You, and Y.-H. Park, "Interfacial bond strength of glass fiber reinforced polymer bars in high-strength concrete," *Compos B Eng*, vol. 39, no. 2, pp. 258–270, 2008.
[18] D. Zhao, J. Pan, Y. Zhou, L. Sui, and Z. Ye, "New types of steel-FRP composite bar with round steel bar inner core: Mechanical properties and bonding performances in concrete," *Constr Build Mater*, vol. 242, May 2020, doi: 10.1016/j.conbuildmat.2020.118062.
[19] S. Han, A. Zhou, and J. Ou, "Relationships between interfacial behavior and flexural performance of hybrid steel-FRP composite bars reinforced seawater sea-sand concrete beams," *Compos Struct*, vol. 277, p. 114672, 2021.
[20] L. Wang, Z. Song, C. Huang, L. Ma, and F. Fu, "Flexural capacity of steel-FCB bar-reinforced coral concrete beams," *Structural Concrete*, vol. 21, no. 6, pp. 2722–2735, 2020.
[21] S. Sun, L. Xing, P. Gui, B. Li, H. Li, L. Zhao, and K. Mei, "Experimental Study on the Bond Performance of Steel–Basalt Fiber Composite Bars in Concrete," *Journal of Composites for Construction*, vol. 27, no. 2, 2023.
[22] M. AlHamaydeh and M. A. Orabi, "Experimental quantification of punching shear capacity for large-scale GFRP-reinforced flat slabs made of synthetic fiber-reinforced self-compacting concrete dataset," *Data Brief*, vol. 37, p. 107196, Aug. 2021, doi: 10.1016/J.DIB.2021.107196.
[23] M. AlHamaydeh and F. M. Amin, "Strength curve data for slender geopolymer concrete columns with GFRP, steel and hybrid reinforcement," *Data Brief*, vol. 39, Dec. 2021, doi: 10.1016/J.DIB.2021.107589.
[24] M. Alhamaydeh and F. Amin, "Data for Interaction Diagrams of Geopolymer FRC Slender Columns with Double-Layer GFRP and Steel Reinforcement," *Data 2021, Vol. 6, Page 43*, vol. 6, no. 5, p. 43, Apr. 2021, doi: 10.3390/DATA6050043.
[25] M. Alhamaydeh and F. Amin, "Data for interaction diagrams of geopolymer frc slender columns with double-layer gfrp and steel reinforcement," *Data (Basel)*, vol. 6, no. 5, May 2021, doi: 10.3390/DATA6050043.
[26] G. Tiberti, I. Trabucchi, M. AlHamaydeh, F. Minelli, and G. A. Plizzari, "Crack development in steel-fibre-reinforced concrete members with conventional rebars," *Magazine of Concrete Research*, vol. 71, no. 11, pp. 599–610, Jun. 2019, doi: 10.1680/JMACR.17.00361.
[27] M. AlHamaydeh, F. Abed, and A. Mustapha, "Key parameters influencing performance and failure modes for BRBs using nonlinear FEA," *J Constr Steel Res*, vol. 116, pp. 1–18, Jan. 2016, doi: 10.1016/j.jcsr.2015.08.038.
[28] M. Alhamaydeh, G. Markou, and D. Saadi, "NONLINEAR FEA OF SOIL-STRUCTURE-INTERACTION EFFECTS ON RC SHEAR WALL STRUCTURES," pp. 3476–3490, 2017, doi: 10.7712/120117.5659.18218.
[29] Y. Wang, M. Wang, X. Zhang, and G. Cai, "Bond of steel-FRP composite bar embedded in FRP-confined concrete: Behavior, mechanism, and strength model," *Eng Struct*, vol. 318, Nov. 2024, doi: 10.1016/j.engstruct.2024.118693.
[30] E. Hognestad, "Study of combined bending and axial load in reinforced concrete members," *University of Illinois. Engineering Experiment Station. Bulletin ; no. 399*, 1951.
[31] T. T. C. . Hsu and Y. L. . Mo, "Unified theory of concrete structures," 2010.
[32] L. Xu, X. Wang, J. Pan, J. Zhou, and W. Liu, "Bond behavior between steel-FRP composite bars and engineered cementitious composites in pullout conditions," *Eng Struct*, vol. 299, Jan. 2024, doi: 10.1016/j.engstruct.2023.117086.
[33] M. AlHamaydeh, Y. Awera, and M. Elkafrawy, "Axial Compressive Behavior of Slender Circular Columns Made of Green Concrete and Double Layers of Steel and GFRP Reinforcement," *Journal of Composites for Construction*, vol. 27, no. 6, Dec. 2023, doi: 10.1061/JCCOF2.CCENG-4123.
[34] M. Al Hamaydeh, F. Afghan, R. Mithani, T. Besiso, and H. Al Salim, "Shear strength of circular beams made of geopolymer concrete and reinforced with GFRP rebars," *AIP Conf Proc*, vol. 2297, Dec. 2020, doi: 10.1063/5.0029862.

[35] M. AlHamaydeh and M. Anwar Orabi, "Punching Shear Behavior of Synthetic Fiber–Reinforced Self-Consolidating Concrete Flat Slabs with GFRP Bars," *Journal of Composites for Construction*, vol. 25, no. 4, p. 04021029, Aug. 2021, doi: 10.1061/(ASCE)CC.1943-5614.0001131/ASSET/D544F241-6509-4DAF-9DCA-8CC6CAF45A55/ASSETS/IMAGES/LARGE/CCENG-3398F13.JPG.

[36] F. Abed, H. El-Chabib, and M. Alhamaydeh, "Shear characteristics of GFRP-reinforced concrete deep beams without web reinforcement," *Journal of Reinforced Plastics and Composites*, vol. 31, no. 16, pp. 1063–1073, Aug. 2012, doi: 10.1177/0731684412450350.

[37] A. Alhayek, A. Syamsir, V. Anggraini, A. Alhayek, A. Syamsir, V. Anggraini, Z. C. Muda, and N. M. Nor, "Design Enhancement of Sustainable Glass Fiber Reinforced Polymer (GFRP) Cross Arm," 2020.

[38] G. Markou and M. Alhamaydeh, "3D Finite Element Modeling of GFRP-Reinforced Concrete Deep Beams without Shear Reinforcement," *Int J Comput Methods*, vol. 15, no. 2, Mar. 2018, doi: 10.1142/S0219876218500019.

[39] M. E. Elkafrawy, A. Mohsen Khalil, W. Abuzaid, R. A. Hawileh, and M. Alhamaydeh, "Nonlinear Finite Element Analysis (NLFEA) of Pre-stressed RC Beams Reinforced with Iron-Based Shape Memory Alloy (Fe-SMA)," *2022 Advances in Science and Engineering Technology International Conferences, ASET 2022*, 2022, doi: 10.1109/ASET53988.2022.9735110.

[40] A. Khalil, M. Elkafrawy, R. Hawileh, and M. Alhamaydeh, "Numerical Investigation on Improving Shear Strength of RC Beams with Various Web Opening Shapes Using Pre-Stressed Fe-SMA Bars," *Key Eng Mater*, vol. 1004, pp. 13–22, 2024, doi: 10.4028/P-E2XIEV.

[41] M. AlHamaydeh and F. M. Amin, "Strength curve data for slender geopolymer concrete columns with GFRP, steel and hybrid reinforcement," *Data Brief*, vol. 39, Dec. 2021, doi: 10.1016/j.dib.2021.107589.

[42] G. Markou and M. AlHamaydeh, "Computationally-efficient high-fidelity nonlinear FEA of seismically isolated post-tensioned RC bridges," *Structures*, vol. 60, Feb. 2024, doi: 10.1016/j.istruc.2023.105816.

[43] M. AlHamaydeh, G. Markou, N. Bakas, and M. Papadrakakis, "AI-based shear capacity of FRP-reinforced concrete deep beams without stirrups," *Eng Struct*, vol. 264, Aug. 2022, doi: 10.1016/j.engstruct.2022.114441.

[44] M. AlHamaydeh and N. Ghazal Aswad, "Structural Health Monitoring Techniques and Technologies for Large-Scale Structures: Challenges, Limitations, and Recommendations," *Practice Periodical on Structural Design and Construction*, vol. 27, no. 3, Aug. 2022, doi: 10.1061/(ASCE)SC.1943-5576.0000703.

[45] M. Elkafrawy, M. AlHamaydeh, H. Zuaiter, and D. ElMaoued, "Improving the Structural Performance of RC Beams with Openings Using Iron-based Shape Memory Alloy (Fe-SMA) Reinforcement," *Procedia Structural Integrity*, vol. 64, pp. 436–444, 2024, doi: 10.1016/J.PROSTR.2024.09.280.